Available online at www.sciencedirect.com
ScienceDirect
Journal of Solid State Chemistry 179 (2006) 3653–3663
JOURNAL OF SOLID STATE CHEMISTRY
www.elsevier.com/locate/jssc

Syntheses, structures, and vibrational spectroscopy of the two-dimensional iodates $Ln(IO_3)_3$ and $Ln(IO_3)_3(H_2O)$ (Ln = Yb, Lu)

Zerihun Assefa[a,b,1], Jie Ling[c], Richard G. Haire[b], Thomas E. Albrecht-Schmitt[c], Richard E. Sykora[b,d,*]

[a]Department of Chemistry, North Carolina A&T State University, Greensboro, NC 27411, USA
[b]Chemical Sciences Division, Oak Ridge National Laboratory, Oak Ridge, TN 37831, USA
[c]Department of Chemistry and Biochemistry, Auburn University, Auburn, AL 36849, USA
[d]Department of Chemistry, University of South Alabama, Mobile, AL 36688, USA

Received 14 June 2006; received in revised form 27 July 2006; accepted 29 July 2006
Available online 4 August 2006

Abstract

The reaction of Lu^{3+} or Yb^{3+} and H_5IO_6 in aqueous media at 180 °C leads to the formation of $Yb(IO_3)_3(H_2O)$ or $Lu(IO_3)_3(H_2O)$, respectively, while the reaction of Yb metal with H_5IO_6 under similar reaction conditions gives rise to the anhydrous iodate, $Yb(IO_3)_3$. Under supercritical conditions Lu^{3+} reacts with HIO_3 and KIO_4 to yield the isostructural $Lu(IO_3)_3$. The structures have been determined by single-crystal X-ray diffraction. Crystallographic data are (Mo$K\alpha$, $\lambda = 0.71073$ Å): $Yb(IO_3)_3$, monoclinic, space group $P2_1/n$, $a = 8.6664(9)$ Å, $b = 5.9904(6)$ Å, $c = 14.8826(15)$ Å, $\beta = 96.931(2)°$, $V = 766.99(13)$, $Z = 4$, $R(F) = 4.23\%$ for 114 parameters with 1880 reflections with $I > 2\sigma(I)$; $Lu(IO_3)_3$, monoclinic, space group $P2_1/n$, $a = 8.6410(9)$, $b = 5.9961(6)$, $c = 14.8782(16)$ Å, $\beta = 97.028(2)°$, $V = 765.08(14)$, $Z = 4$, $R(F) = 2.65\%$ for 119 parameters with 1756 reflections with $I > 2\sigma(I)$; $Yb(IO_3)_3(H_2O)$, monoclinic, space group $C2/c$, $a = 27.2476(15)$, $b = 5.6296(3)$, $c = 12.0157(7)$ Å, $\beta = 98.636(1)°$, $V = 1822.2(2)$, $Z = 8$, $R(F) = 1.51\%$ for 128 parameters with 2250 reflections with $I > 2\sigma(I)$; $Lu(IO_3)_3(H_2O)$, monoclinic, space group $C2/c$, $a = 27.258(4)$, $b = 5.6251(7)$, $c = 12.0006(16)$ Å, $\beta = 98.704(2)°$, $V = 1818.8(4)$, $Z = 8$, $R(F) = 1.98\%$ for 128 parameters with 2242 reflections with $I > 2\sigma(I)$. The f elements in all of the compounds are found in seven-coordinate environments and bridged with monodentate, bidentate, or tridentate iodate anions. Both $Lu(IO_3)_3(H_2O)$ and $Yb(IO_3)_3(H_2O)$ display distinctively different vibrational profiles from their respective anhydrous analogs. Hence, the Raman profile can be used as a complementary diagnostic tool to discern the different structural motifs of the compounds.

Keywords: Lutetium iodate; Ytterbium iodate; Hydrothermal; Single-crystal X-ray diffraction; Raman spectroscopy; Layered compounds; Structure determination

1. Introduction

Lanthanide iodates have been studied for their nonlinear optical properties including second harmonic generation [1], and have been shown to exhibit piezoelectric [2] and pyroelectric effects [3,4]. In attempts to prepare acentric structures of lanthanide iodates, no less than six anhydrous structure types have been reported [1], in addition to numerous hydrated structures ranging from hemihydrates to pentahydrates [1,5]. The known structure type that incorporates the broadest range of trivalent rare earth elements is the type I $Ln(IO_3)_3$ structure, which has been reported for Ce–Lu (except Pm), [1,6] Y [1], Am [7], and Cm [8]. Structural data for many of the iodates have been limited by the inability to grow single crystals. Single-crystal X-ray diffraction has been used to determine the structures of several anhydrous [6–10] and hydrated [4,5,11–13] trivalent f-element iodates.

*Corresponding author at Department of Chemistry, University of South Alabama, 307 University Boulevard, Mobile, AL 36688, USA. Fax: +251 460 7359.
E-mail addresses: zassefa@ncat.edu (Z. Assefa), rsykora@jaguar1.usouthal.edu (R.E. Sykora).
[1]Also for correspondence at Department of Chemistry, North Carolina A&T State University, New Science Building, Greensboro, NC 27411, USA. Fax: +336 334 7124.

0022-4596/$ - see front matter © 2006 Elsevier Inc. All rights reserved.
doi:10.1016/j.jssc.2006.07.042

We have recently begun studying the iodates of the trivalent 5*f* elements [7,8,10]. While the chemistry of the lanthanide iodates is fueled by the search for novel optoelectronic materials, the actinide iodates are of interest regarding their radiation stability [7,8,14] and their low solubilities, where the latter can be utilized in chemical separations [15–17]. We have shown that one can prepare the Type I $Ln(IO_3)_3$ structure type with Am [7] and Cm [8], but the $Bi(IO_3)_3$ structure type [18] is formed with the smaller Cf ion [10]. With the earlier actinide elements, uranium through plutonium, structural data only exist for the iodates with the high-valent states of the actinides, e.g. $UO_2(IO_3)_2$ [19], $NpO_2(IO_3)$ [20], and $PuO_2(IO_3)_2 \cdot H_2O$ [21].

To aid our systematic studies of the actinide iodates it is desirable to draw comparisons with their lanthanide analogs and lanthanide elements are often used as models for the rarer and radioactive actinide elements. While working out schemes for preparing single crystals of the smaller trivalent actinide iodates, we prepared a new structure type for the iodates that has not been previously reported. Herein we report the syntheses, structures, and Raman spectroscopy for a new lanthanide iodate structural family containing the lanthanide elements with the smallest radii, $Ln(IO_3)_3(H_2O)$ (Ln = Yb, Lu). In addition, we have isolated single crystals of $Yb(IO_3)_3$ and $Lu(IO_3)_3$ that adopt the $Bi(IO_3)_3$ structure type [18], and have also characterized them using single-crystal X-ray diffraction and Raman spectroscopy.

2. Experimental

2.1. Materials

$Lu(NO_3)_3 \cdot xH_2O$ (99.9%, Alfa Aesar), $Yb(NO_3)_3 \cdot xH_2O$ (99.9%, Research Chemicals), Yb metal (99+%, Cerac), KIO_4 (99.8%, Alfa Aesar), HIO_3 (99.5%, Alfa Aesar), and H_5IO_6 (98%, Alfa Aesar) were used as received without further purification. Distilled and Millipore filtered water was used in all reactions. The reactions reported here produced the highest yield of the respective compounds.

2.2. Synthesis of $Yb(IO_3)_3$

The synthesis of $Yb(IO_3)_3$ involved loading Yb metal filings (3.92 mg, 22.7 μmol) and H_5IO_6 (19.5 mg, 85.6 μmol) into a quartz ampoule followed by the addition of water (0.10 mL). The ampoule was flame sealed and placed in a box furnace that had been preheated to 180 °C. After 70 h the furnace was turned off and allowed to self-quench to 20 °C. The sole crystalline product, $Yb(IO_3)_3$, was isolated in the form of colorless irregularly shaped crystals located beneath a colorless mother liquor.

2.3. Synthesis of $Lu(IO_3)_3$

$Lu(NO_3)_3 \cdot xH_2O$ (77.0 mg, 0.213 mmol), KIO_4 (98.1 mg, 0.426 mmol), and HIO_3 (75.0 mg, 0.426 mmol) were loaded into a quartz ampoule (1.15 mL volume) along with 150 μL of water. The ampoule was frozen and sealed under vacuum. After thawing, the ampoule was placed in a Leco Tem-Press 27-mL autoclave filled with water and counter pressured with 2500 psi of argon. The autoclave was heated to 425 °C, where it was held for three days and then slow cooled to 25 °C at the rate of 1 °C/h. The product consisted of colorless columnar needles of $Lu(IO_3)_3$.

2.4. Synthesis of $Yb(IO_3)_3(H_2O)$ and $Lu(IO_3)_3(H_2O)$

The synthesis of $Yb(IO_3)_3(H_2O)$ involved mixing $Yb(NO_3)_3$ (126 μL, 0.1 M) and H_5IO_6 (8.63 mg, 37.9 μmol) in a 1 mL quartz reaction vessel. The reaction vessel was sealed, placed in a box furnace, and then heated to 180 °C where the reaction occurred under autogenously generated pressure. After 88 h the furnace was cooled at 10 °C/h to 100 °C, then turned off and allowed to self-quench to 20 °C. The sole solid product was colorless single crystals of $Yb(IO_3)_3(H_2O)$ submersed in a colorless mother liquor. The synthesis of $Lu(IO_3)_3(H_2O)$ involved mixing $Lu(NO_3)_3$ (20 μL, 0.1 M) and H_5IO_6 (60 μL, 0.1 M) in a quartz reaction vessel. The reaction vessel was sealed and placed in a box furnace and then heated to 180 °C where the reaction occurred under autogenously generated pressure. After 67 h the furnace was cooled at 20 °C/h to 100 °C, then turned off and self-quenched to 20 °C. The obtained product was colorless single crystals of $Lu(IO_3)_3(H_2O)$ beneath a colorless mother liquor.

2.5. Crystallographic studies

Crystals of $Yb(IO_3)_3$, $Lu(IO_3)_3$, $Yb(IO_3)_3(H_2O)$, and $Lu(IO_3)_3(H_2O)$ with dimensions of 0.136 mm × 0.064 mm × 0.042 mm, 0.064 mm × 0.028 mm × 0.027 mm, 0.456 mm × 0.072 mm × 0.012 mm, and 0.570 mm × 0.080 mm × 0.010 mm, respectively, were selected, mounted on quartz fibers with epoxy, and aligned on a Bruker SMART APEX CCD X-ray diffractometer with a digital camera. Intensity measurements were performed using graphite monochromated Mo$K\alpha$ radiation from a sealed tube with a monocapillary collimator. The intensities and positions of reflections of a sphere were collected by a combination of three sets of exposure frames. Each set had a different φ angle for the crystal and each exposure covered a range of 0.3° in ω. A total of 1800 frames were collected with an exposure time per frame of 20 s for $Yb(IO_3)_3(H_2O)$, $Lu(IO_3)_3(H_2O)$, and $Yb(IO_3)_3$ and 30 s for $Lu(IO_3)_3$.

Determination of integrated intensities and global cell refinement were performed with the Bruker SAINT (v 6.02) software package using a narrow-frame integration algorithm. An analytical absorption correction was applied based on the indexed crystal faces followed by a

semi-empirical absorption correction using SADABS [22]. The program suite SHELXTL (v 5.1) was used for space group determination (XPREP), direct methods structure solution (XS), and least-squares refinement (XL) [23]. The final refinements included anisotropic displacement parameters for all atoms and a secondary extinction parameter. Some crystallographic details are listed in Table 1 and the final positional parameters can be found in Tables 2–5. Further details of the crystal structure investigations may be obtained from the Fachinformationzentrum Karlsruhe, D-76344 Eggenstein-Leopoldshafen, Germany (Fax: (+49)7247-808-666; Email: crysdata@fiz-karlsruhe.de) on quoting the depository numbers CSD 416690, 416691, 416692, and 416693 for $Yb(IO_3)_3$, $Lu(IO_3)_3$, $Yb(IO_3)_3(H_2O)$, and $Lu(IO_3)_3(H_2O)$, respectively.

2.6. Raman spectroscopy

Raman spectroscopic experiments were performed using an argon-ion laser (Coherent, model 306) and a double-meter spectrometer (Jobin-Yvon Ramanor model HG.2S). As a double-meter spectrometer, the Ramanor has a total of four slits (one entrance, one exit and two internal slits) that are manually controlled. Based on the manufacturer's calibration, the maximum resolution for the monochromator at 514.5 nm is 0.5 cm^{-1}. However, the resolution for the spectra reported here varies from sample to sample. In fact the signal intensity is a function of four factors: the applied laser power, the sample properties (how absorptive/reflective the sample is and the intrinsic strength of the Raman modes), and the widths of the spectrometer's entrance and exit slits. Some tradeoff was attained between

Table 1
Crystallographic data for $Yb(IO_3)_3(H_2O)$, $Lu(IO_3)_3(H_2O)$, $Yb(IO_3)_3$, and $Lu(IO_3)_3$

Compound	$Yb(IO_3)_3(H_2O)$	$Lu(IO_3)_3(H_2O)$	$Yb(IO_3)_3$	$Lu(IO_3)_3$
Formula mass (amu)	715.76	717.69	697.74	699.67
Color and habit	Colorless, plate	Colorless, plate	Colorless, prism	Colorless, needle
Crystal system	Monoclinic	Monoclinic	Monoclinic	Monoclinic
Space group	$C2/c$ (no. 15)	$C2/c$ (no. 15)	$P2_1/n$ (no. 14)	$P2_1/n$ (no. 14)
a (Å)	27.2476(15)	27.258(4)	8.6664(9)	8.6410(9)
b (Å)	5.6296(3)	5.6251(7)	5.9904(6)	5.9961(6)
c (Å)	12.0157(7)	12.0006(16)	14.8826(15)	14.8782(16)
β	98.636(1)	98.704(2)	96.931(2)	97.028(2)
V (Å^3)	1822.2(2)	1818.8(4)	766.99(13)	765.08(14)
Z	8	8	4	4
T (K)	173	173	173	193
λ (Å)	0.71073	0.71073	0.71073	0.71073
$2\theta_{max}$	56.58	56.64	56.64	56.54
ρ_{calcd} (g cm^{-3})	5.218	5.242	6.042	6.074
μ(Mo$K\alpha$) (cm^{-1})	204.66	210.76	242.94	250.34
$R(F)$ for $F_o^2 > 2\sigma(F_o^2)$[a]	0.0151	0.0198	0.0423	0.0239
$R_w(F_o^2)$[b]	0.0345	0.0523	0.1341	0.0541

[a] $R(F) = \sum||F_o| - |F_c||/\sum|F_o|$.
[b] $R_w(F_o^2) = \left[\sum\left[w(F_o^2 - F_c^2)^2\right]/\sum wF_o^4\right]^{1/2}$.

Table 2
Atomic coordinates and equivalent isotropic displacement parameters for $Yb(IO_3)_3$

Atom	Site	x	y	z	U_{eq} (Å^2)[a]
Yb(1)	4e	0.5419(1)	0.7197(1)	0.8948(1)	0.007(1)
I(1)	4e	0.8320(1)	0.3500(2)	0.9795(1)	0.006(1)
I(2)	4e	0.6175(1)	0.4060(2)	0.6985(1)	0.006(1)
I(3)	4e	0.2809(1)	0.1926(2)	0.8558(1)	0.006(1)
O(1)	4e	0.7698(15)	0.5290(20)	0.8831(9)	0.010(3)
O(2)	4e	0.3627(16)	0.6350(20)	0.9861(9)	0.012(3)
O(3)	4e	0.9108(15)	0.5630(20)	0.0615(9)	0.010(3)
O(4)	4e	0.5852(15)	0.6840(20)	0.7434(8)	0.008(2)
O(5)	4e	0.4588(17)	0.4160(30)	0.6090(10)	0.015(3)
O(6)	4e	0.7770(16)	0.4930(20)	0.6363(8)	0.011(3)
O(7)	4e	0.3693(16)	0.9470(20)	0.8110(9)	0.012(3)
O(8)	4e	0.3558(15)	0.1350(20)	0.9714(9)	0.012(3)
O(9)	4e	0.4223(15)	0.4000(20)	0.8289(10)	0.012(3)

[a] U_{eq} is defined as one-third of the trace of the orthogonalized $\mathbf{U}_{ij}$ tensor.

Table 3
Atomic coordinates and equivalent isotropic displacement parameters for $Lu(IO_3)_3$

Atom	Site	x	y	z	U_{eq} (Å^2)[a]
Lu(1)	4*e*	0.5418(1)	0.7186(1)	0.8940(1)	0.008(1)
I(1)	4*e*	0.8316(1)	0.3495(1)	0.9797(1)	0.007(1)
I(2)	4*e*	0.6176(1)	0.4061(1)	0.6983(1)	0.008(1)
I(3)	4*e*	0.2814(1)	0.1930(1)	0.8566(1)	0.008(1)
O(1)	4*e*	0.7694(5)	0.5287(7)	0.8830(3)	0.012(1)
O(2)	4*e*	0.3630(5)	0.6384(8)	0.9856(3)	0.016(1)
O(3)	4*e*	0.9098(5)	0.5600(7)	0.0613(3)	0.011(1)
O(4)	4*e*	0.5853(5)	0.6821(7)	0.7430(3)	0.010(1)
O(5)	4*e*	0.4557(5)	0.4157(8)	0.6091(3)	0.016(1)
O(6)	4*e*	0.7774(5)	0.4912(7)	0.6359(3)	0.011(1)
O(7)	4*e*	0.3727(5)	0.9492(7)	0.8126(3)	0.013(1)
O(8)	4*e*	0.3516(5)	0.1339(8)	0.9729(3)	0.014(1)
O(9)	4*e*	0.4215(5)	0.4021(7)	0.8297(3)	0.013(1)

[a] U_{eq} is defined as one-third of the trace of the orthogonalized $\mathbf{U}_{ij}$ tensor.

Table 4
Atomic coordinates and equivalent isotropic displacement parameters for $Yb(IO_3)_3(H_2O)$

Atom	Site	x	y	z	U_{eq} (Å^2)[a]
Yb(1)	8*f*	0.0835(1)	0.2058(1)	0.4311(1)	0.008(1)
I(1)	8*f*	0.2145(1)	0.1905(1)	0.3479(1)	0.008(1)
I(2)	8*f*	0.1669(1)	0.7413(1)	0.5587(1)	0.007(1)
I(3)	8*f*	0.0933(1)	0.7010(1)	0.2367(1)	0.008(1)
O(1)	8*f*	0.1561(1)	0.0646(4)	0.3798(2)	0.013(1)
O(2)	8*f*	0.2183(1)	0.0181(5)	0.2227(2)	0.014(1)
O(3)	8*f*	0.2560(1)	0.0195(5)	0.4490(2)	0.017(1)
O(4)	8*f*	0.1362(1)	0.5342(5)	0.4539(2)	0.014(1)
O(5)	8*f*	0.1147(1)	0.9414(5)	0.5654(2)	0.013(1)
O(6)	8*f*	0.1609(1)	0.5715(4)	0.6835(2)	0.012(1)
O(7)	8*f*	0.0600(1)	0.6761(5)	0.0950(2)	0.013(1)
O(8)	8*f*	0.0571(1)	0.9265(4)	0.2951(2)	0.015(1)
O(9)	8*f*	0.0637(1)	0.4414(2)	0.2835(2)	0.014(1)
O(10)	8*f*	−0.0028(1)	0.1986(5)	0.4043(2)	0.015(1)

[a] U_{eq} is defined as one-third of the trace of the orthogonalized $\mathbf{U}_{ij}$ tensor.

Table 5
Atomic coordinates and equivalent isotropic displacement parameters for $Lu(IO_3)_3(H_2O)$

Atom	Site	x	y	z	U_{eq} (Å^2)[a]
Lu(1)	8*f*	0.0835(1)	0.2056(1)	0.4302(1)	0.007(1)
I(1)	8*f*	0.2143(1)	0.1905(1)	0.3475(1)	0.008(1)
I(2)	8*f*	0.1667(1)	0.7399(1)	0.5580(1)	0.007(1)
I(3)	8*f*	0.0933(1)	0.7011(1)	0.2362(1)	0.008(1)
O(1)	8*f*	0.1558(1)	0.0635(5)	0.3788(2)	0.012(1)
O(2)	8*f*	0.2183(1)	0.0188(6)	0.2216(2)	0.013(1)
O(3)	8*f*	0.2557(1)	0.0179(6)	0.4484(2)	0.017(1)
O(4)	8*f*	0.1361(1)	0.5302(6)	0.4536(2)	0.013(1)
O(5)	8*f*	0.1143(1)	0.9387(6)	0.5637(2)	0.013(1)
O(6)	8*f*	0.1609(1)	0.5705(5)	0.6829(2)	0.012(1)
O(7)	8*f*	0.0601(1)	0.6775(5)	0.0939(2)	0.013(1)
O(8)	8*f*	0.0572(1)	0.9273(6)	0.2953(2)	0.014(1)
O(9)	8*f*	0.0634(1)	0.4411(5)	0.2828(2)	0.013(1)
O(10)	8*f*	−0.0024(1)	0.1976(6)	0.4044(3)	0.016(1)

[a] U_{eq} is defined as one-third of the trace of the orthogonalized $\mathbf{U}_{ij}$ tensor.

the resolving power and intensity of the Raman signal. In some cases the excitation wavelength was also changed to optimize the signal. The 528.7 nm green laser line was the principal excitation source that provided optimal signal for most of the samples. Hence, the resolution of each spectrum reported in this manuscript is different from the maximum attainable value. The actual resolution of the Raman signal for the samples varied between 1 and 2 cm^{-1}. Most of the spectra were collected at dwell time of 0.5 s/pt, and the signal detection was acquired using a water-cooled photo-multiplier tube (Hamamatsu R636). The analog signal from the PMT was digitized using an ADC interfaced with the instrument and the data stored in a personal computer. The LabSpec (version 3.04) software controlled scanning and other instrumental functions. The samples were all crystalline, and the Raman data were performed on capillary tubes compacted with these crystalline materials. Hence, the sample orientation is random and a polarizer was not used on either the incident radiation or the collection of the Raman signal scattered from the sample. We are, thus, unable to address any polarization effect. The Raman collection lens and the monochromater entrance slit were positioned at 90° to the incident radiation. The reported spectra are uncorrected for any instrumental responses. However, the monochromator positions and wavenumber accuracies were calibrated daily using the sharp Hg line at 18312.7 cm^{-1} (546.1 nm) using a fluorescent lamp. Additional calibration was conducted using the tri-azaphospha-adamantane ligand; several sharp and strong Raman bands in the region of interest were used as standards.

3. Results and discussion

3.1. Syntheses

The reactions of 0.1 M ytterbium or lutetium nitrate solutions with periodic acid at 180 °C leads to the formation of $Yb(IO_3)_3(H_2O)$ and $Lu(IO_3)_3(H_2O)$ single crystals, respectively, in the form of colorless tablets. This reaction involves the reduction of the periodate to form iodate and the simultaneous oxidation of H_2O to oxygen and H^+. This reduction of periodate to iodate has been previously noted under similar synthetic conditions [7,19].

Type I $Ln(IO_3)_3$ iodates have been reported for Ce–Lu [1], Y [1], Am [7], and Cm [8]. The reaction of the larger trivalent *f*-element ions with H_5IO_6 under mild hydrothermal conditions produces the Type I iodate phase [7,8]. For the smallest trivalent lanthanide ions, Yb^{3+} and Lu^{3+}, the hydrothermal reaction reported here produces $Ln(IO_3)_3(H_2O)$ (Ln = Yb, Lu). The formation of $Yb(IO_3)_3 \cdot 2H_2O$ and $Lu(IO_3)_3 \cdot 2H_2O$ have been previously reported [11,12] by reacting the appropriate amorphous lanthanide periodate with excess periodic acid in aqueous solution at 160 °C. We have been successful in preparing $Yb(IO_3)_3$, containing the $Bi(IO_3)_3$ structure type [18], by reacting Yb metal with H_5IO_6 under hydrothermal conditions. Under these conditions, H_5IO_6 presumably oxidizes both Yb and H_2O. Only by using supercritical conditions (425 °C) have we been able to grow crystals of the anhydrous lutetium iodate, $Lu(IO_3)_3$.

3.2. Structures

3.2.1. Structures of $Yb(IO_3)_3$ and $Lu(IO_3)_3$

The anhydrous iodates $Yb(IO_3)_3$ and $Lu(IO_3)_3$ adopt the $Bi(IO_3)_3$ structure type [18]. Surprisingly, the larger Nd^{3+} cation can also be induced to form crystals in this class [9]. We have also recently shown that $Cf(IO_3)_3$ conforms to this crystal system as well [10]. Since $Yb(IO_3)_3$ and $Lu(IO_3)_3$ are isostructural, below we only discuss the structure of $Lu(IO_3)_3$; the structural features found in $Yb(IO_3)_3$ are the same as that for $Lu(IO_3)_3$, with only slight variations in bond distances and angles.

The most distinctive feature of this structure is the environment of the M^{3+} cations. These cations are situated in monocapped trigonal prismatic environments with Lu–O bond distances ranging from 2.234(4) to 2.341(4) Å. In addition to these seven contacts, there are two much longer Lu···O interactions of 2.847(5) and 3.279(5) Å that cap two additional faces of the trigonal prism. The local environment of the Lu^{3+} cation is shown in Fig. 1 and the overall structure of $Lu(IO_3)_3$ is two dimensional as shown in Fig. 2. However, there is an unusual one-dimensional substructure that consists of chains of LuO_7 polyhedra and iodate anions. The LuO_7 units edge share to yield a Lu···Lu distance of 4.230(5) Å. There are three crystallographically unique iodine atoms in $Lu(IO_3)_3$, where the I–O bond distances are normal and range from 1.797(4) to 1.828(4) Å. The O–I–O bond angles show significant variations, and range from 90.4(2) to

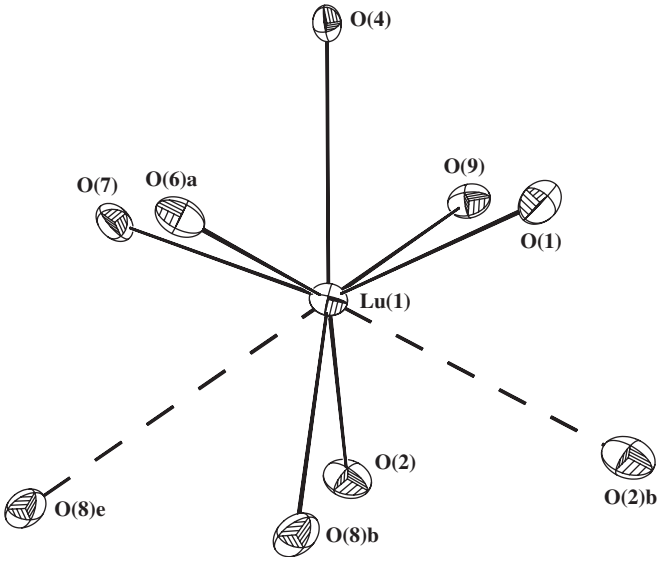

Fig. 1. The coordination environment of the Lu site in $Lu(IO_3)_3$ (50% probability ellipsoids are shown). Operations used to generate symmetry equivalent atoms: (a) 1.5−*x*, 0.5+*y*, 1.5−*z*; (b) 1−*x*, 1−*y*, 2−*z*; (e) *x*, 1+*y*, *z*.

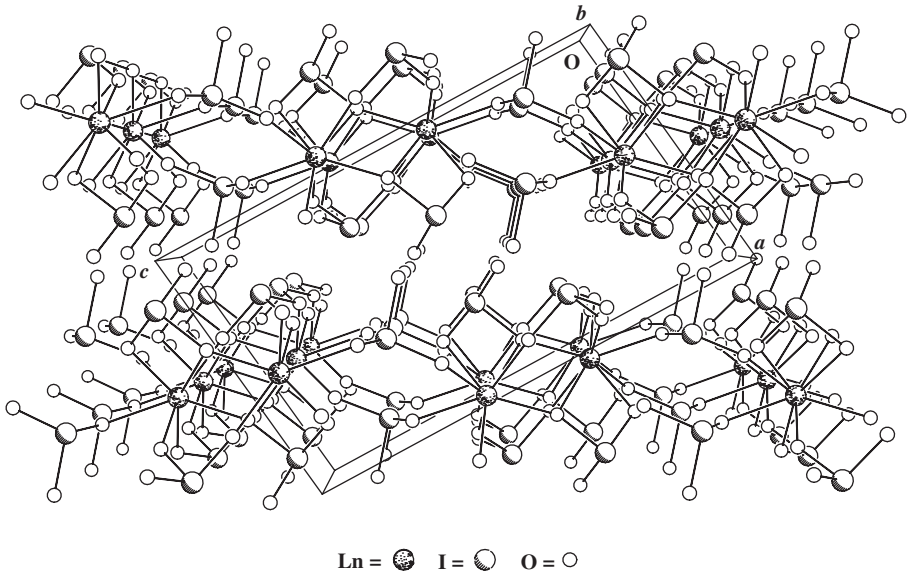

Fig. 2. A packing diagram viewed along the *b*-axis showing the stacking of the two-dimensional layers in $Ln(IO_3)_3$ (Ln = Yb, Lu).

Table 6
Bond distances (Å) and angles (deg) for $Yb(IO_3)_3$

Bond distances (Å)			
Yb(1)–O(1)	2.306(13)	I(1)–O(2)b	1.823(13)
Yb(1)–O(2)	2.241(13)	I(1)–O(3)c	1.841(13)
Yb(1)–O(4)	2.338(12)	I(2)–O(4)	1.830(13)
Yb(1)–O(6)a	2.351(14)	I(2)–O(5)	1.797(14)
Yb(1)–O(7)	2.279(14)	I(2)–O(6)	1.830(13)
Yb(1)–O(8)b	2.254(13)	I(3)–O(7)d	1.823(14)
Yb(1)–O(9)	2.341(4)	I(3)–O(8)	1.798(13)
I(1)–O(1)	1.819(14)	I(3)–O(9)	1.822(13)
Angles (deg)			
O(1)–I(1)–O(2)b	89.8(6)	O(4)–I(2)–O(6)	94.8(6)
O(1)–I(1)–O(3)c	99.5(6)	O(7)d–I(3)–O(8)	94.4(6)
O(2)b–I(1)–O(3)c	93.6(6)	O(7)d–I(3)–O(9)	98.5(6)
O(4)–I(2)–O(5)	96.0(6)	O(8)–I(3)–O(9)	99.6(6)
O(5)–I(2)–O(6)	99.9(6)		

Symmetry codes: (a) $3/2-x$, $1/2+y$, $3/2-z$; (b) $1-x$, $1-y$, $2-z$; (c) x, y, $1+z$; (d) x, $y-1$, z.

Table 7
Bond distances (Å) and angles (deg) for $Lu(IO_3)_3$

Bond distances (Å)			
Lu(1)–O(1)	2.295(4)	I(1)–O(2)b	1.820(4)
Lu(1)–O(2)	2.234(4)	I(1)–O(3)c	1.823(4)
Lu(1)–O(4)	2.333(4)	I(2)–O(4)	1.818(4)
Lu(1)–O(6)a	2.341(4)	I(2)–O(5)	1.808(4)
Lu(1)–O(7)	2.255(4)	I(2)–O(6)	1.828(4)
Lu(1)–O(8)b	2.260(5)	I(3)–O(7)d	1.820(4)
Lu(1)–O(9)	2.314(4)	I(3)–O(8)	1.797(4)
I(1)–O(1)	1.822(4)	I(3)–O(9)	1.821(4)
Angles (deg)			
O(1)–I(1)–O(2)b	90.4(2)	O(4)–I(2)–O(6)	95.2(2)
O(1)–I(1)–O(3)c	99.6(2)	O(7)d–I(3)–O(8)	94.5(2)
O(2)b–I(1)–O(3)c	93.6(2)	O(7)d–I(3)–O(9)	98.3(2)
O(4)–I(2)–O(5)	95.8(2)	O(8)–I(3)–O(9)	101.1(2)
O(5)–I(2)–O(6)	100.6(2)		

Symmetry codes: (a) $3/2-x$, $1/2+y$, $3/2-z$; (b) $1-x$, $1-y$, $2-z$; (c) x, y, $1+z$; (d) x, $y-1$, z.

101.1(2)°. A detailed list of bond lengths and angles for $Yb(IO_3)_3$ and $Lu(IO_3)_3$ can be found in Tables 6 and 7.

3.2.2. Structures of $Yb(IO_3)_3(H_2O)$ and $Lu(IO_3)_3(H_2O)$

$Yb(IO_3)_3(H_2O)$ and $Lu(IO_3)_3(H_2O)$ are isostructural, and for brevity both structures will be discussed simultaneously. The Ln(1) positions in the structures of both $Yb(IO_3)_3(H_2O)$ and $Lu(IO_3)_3(H_2O)$ are coordinated by six iodate anions and one water molecule giving rise to a LnO_7 coordination polyhedron as shown in Fig. 3. Crystallographically, there are three unique iodine atoms, I(1), I(2), and I(3), in the structure. Each of these iodine atoms is coordinated by three oxygen atoms, in a trigonal pyramidal arrangement, and each possesses a lone pair of electrons. In the structures of $Yb(IO_3)_3(H_2O)$ and $Lu(IO_3)_3(H_2O)$, iodate anions are found to be monodentate, bidentate, and tridentate. Although it is not uncommon for at least two types of iodate coordination to be present in an *f*-element iodate structure [24,25], the presence of three distinct coordination modes is not as prevalent [12]. The iodate anions in $Yb(IO_3)_3(H_2O)$ and $Lu(IO_3)_3(H_2O)$ each contain three different I–O bond distances, and therefore have site symmetries of C_1. This lowering of the expected C_{3v} site symmetry for an isolated iodate anion is very commonly observed in the structures of solid-state iodates.

The iodate ion formed by I(1) is a monodentate ligand that coordinates Ln(1) through O(1) and contains two terminal oxygen atoms, O(2) and O(3). I(2) is found in a bidentate iodate anion that coordinates with O(4) and O(5) and contains one terminal oxygen atom, O(6). The

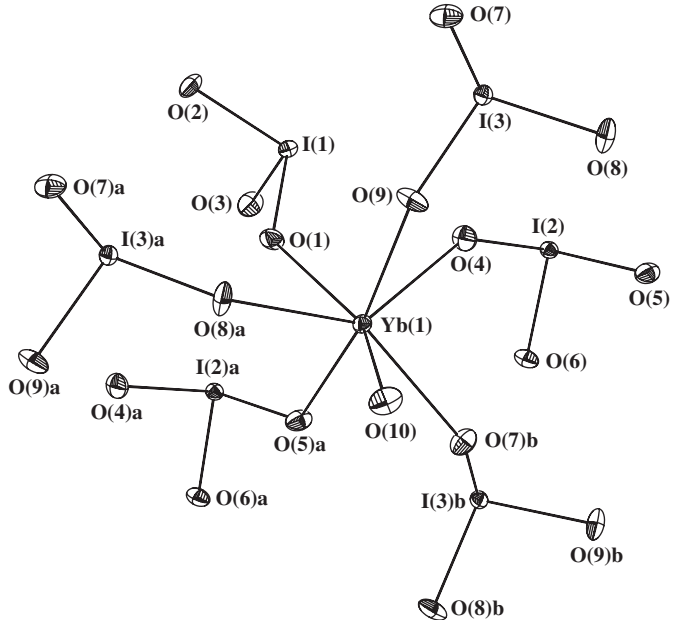

Fig. 3. The coordination environment of the Yb site in $Yb(IO_3)_3(H_2O)$ (50% probability ellipsoids are shown). Operations used to generate symmetry equivalent atoms: (a) x, $y-1$, z; (b) x, $1-y$, $1/2+z$.

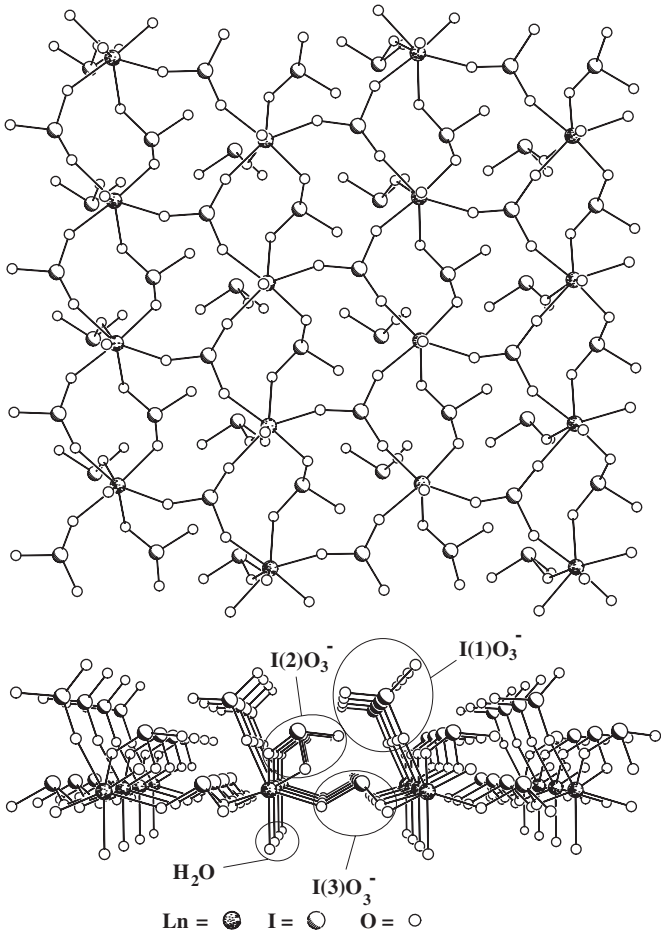

Fig. 4. A ball and stick plot of a two-dimensional layer in $Ln(IO_3)_3(H_2O)$ (Ln = Yb, Lu) viewed (a) perpendicular to the layer or (b) parallel to the layer.

tridentate iodate anion, formed with I(3), coordinates Ln(1) with all three of its oxygen atoms, O(7), O(8), and O(9). Therefore, each Ln(1) position is coordinated with one $I(1)O_3^-$, two $I(2)O_3^-$, and three $I(3)O_3^-$. The seventh and last oxygen atom bonded to Ln(1) is O(10), the oxygen from the coordinated water molecule.

Three LnO_7 polyhedra are linked together by each triply bridging $I(3)O_3^-$ anion, resulting in two-dimensional layers as shown in Fig. 4. The bidentate $I(2)O_3^-$ anions additionally bridge two intralayer LnO_7 polyhedra leading to more rigid layers, while the monodentate $I(1)O_3^-$ anions are all coordinated on one side of each layer. The Ln-coordinated water molecules terminate the opposite side of each layer. These layers stack upon one another and are connected only by noncovalent interactions. The layers alternate in direction so that iodate-terminated and water-terminated sides of the layers interact with one another. This stacking pattern is illustrated in Fig. 5.

The Ln–O bond lengths for the LnO_7 polyhedra range from 2.216(2) to 2.332(2) Å and 2.212(3) to 2.315(3) Å for $Yb(IO_3)_3(H_2O)$ and $Lu(IO_3)_3(H_2O)$, respectively. These distances are within the range found for other iodate structures of these elements [11,12]. The iodate anions have I–O bond lengths ranging from 1.799(2) to 1.838(3) Å, well within the range found for other lanthanide and actinide iodates. In addition, each iodine atom forms two or three longer bonds to oxygen atoms with distances from 2.550(3) to 2.958(3) Å. A detailed list of bond lengths and angles for $Yb(IO_3)_3(H_2O)$ and $Lu(IO_3)_3(H_2O)$ can be found in Tables 8 and 9.

The bond valence sums for all of the atomic positions have been calculated [26]. The values for Yb(3.12) and Lu(3.08) are consistent with Ln(III), while the iodine atoms have average values of 4.96 and 4.94 for $Yb(IO_3)_3(H_2O)$ and $Lu(IO_3)_3(H_2O)$, respectively, and support the assignment of these positions as I(V). The bond valence sums for the oxygen positions of the iodate groups range from 1.68 to 2.26 for $Yb(IO_3)_3(H_2O)$ and 1.67–2.22 for $Lu(IO_3)_3(H_2O)$. The O(10) position, assigned as the coordinated water molecule in both structures, has a bond valence of 0.40 for $Yb(IO_3)_3(H_2O)$ and 0.39 for $Lu(IO_3)_3(H_2O)$ and is consistent with their assignments.

3.3. Raman spectroscopy

3.3.1. Raman spectra of $Lu(IO_3)_3$ and $Yb(IO_3)_3$

In Fig. 6 the Raman spectra of $Lu(IO_3)_3$ and $Yb(IO_3)_3$ are shown in the I–O stretching frequency region. Consistent with the size of the metal ions and structural similarities of the two compounds, the Raman profiles are quite similar in both energy position and relative intensity of the peaks. In the I–O stretching frequency region, the Raman spectrum of $Lu(IO_3)_3$ exhibits three regions with a strong doublet at 699 and 723 cm^{-1}, a broad doublet at 767 and 782 cm^{-1}, and a strong band at 842 cm^{-1} present. The Raman bands of $Yb(IO_3)_3$ exhibit a similar profile and

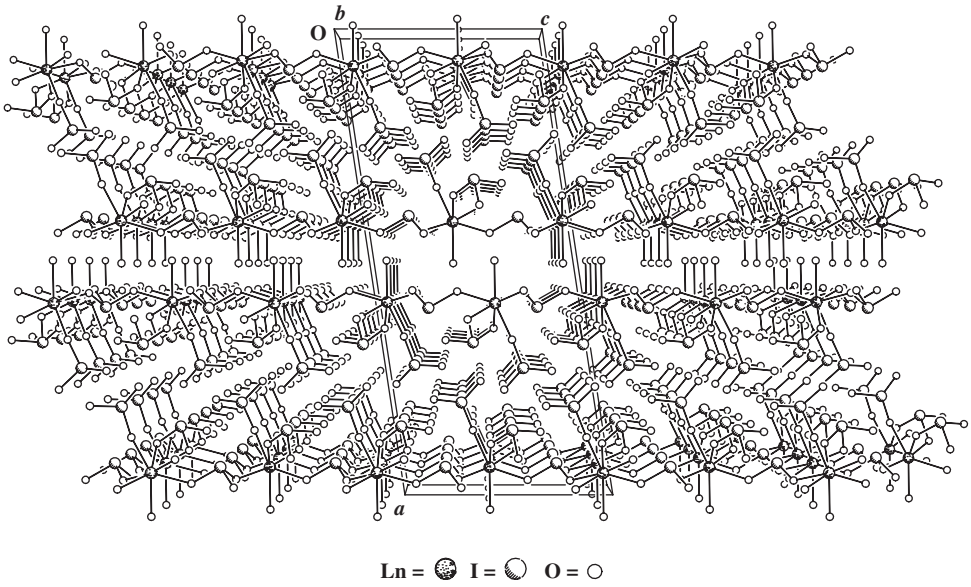

Fig. 5. A packing diagram showing the stacking of the two-dimensional layers in $Ln(IO_3)_3(H_2O)$ (Ln = Yb, Lu).

Table 8
Bond distances (Å) and angles (deg) for $Yb(IO_3)_3(H_2O)$

Bond distances (Å)			
Yb(1)–O(1)	2.301(2)	I(1)–O(2)	1.807(2)
Yb(1)–O(4)	2.332(2)	I(1)–O(3)	1.808(3)
Yb(1)–O(5)a	2.265(2)	I(2)–O(4)	1.824(2)
Yb(1)–O(7)b	2.259(2)	I(2)–O(5)	1.824(2)
Yb(1)–O(8)a	2.303(2)	I(2)–O(6)	1.806(2)
Yb(1)–O(9)	2.216(2)	I(3)–O(7)	1.811(2)
Yb(1)–O(10)	2.325(3)	I(3)–O(8)	1.812(2)
I(1)–O(1)	1.833(2)	I(3)–O(9)	1.799(2)
Angles (deg)			
O(1)–I(1)–O(2)	97.32(12)	O(5)–I(2)–O(6)	97.04(11)
O(1)–I(1)–O(3)	97.37(12)	O(7)–I(3)–O(8)	101.17(12)
O(2)–I(1)–O(3)	99.51(12)	O(7)–I(3)–O(9)	92.63(11)
O(4)–I(2)–O(5)	98.38(12)	O(8)–I(3)–O(9)	98.78(12)
O(4)–I(2)–O(6)	98.37(11)		

Symmetry Codes: (a) x, $y-1$, z; (b) x, $1-y$, $1/2+z$.

Table 9
Bond distances (Å) and angles (deg) for $Lu(IO_3)_3(H_2O)$

Bond distances (Å)			
Lu(1)–O(1)	2.295(3)	I(1)–O(2)	1.810(3)
Lu(1)–O(4)	2.312(3)	I(1)–O(3)	1.807(3)
Lu(1)–O(5)a	2.262(3)	I(2)–O(4)	1.828(3)
Lu(1)–O(7)b	2.254(3)	I(2)–O(5)	1.823(3)
Lu(1)–O(8)a	2.288(3)	I(2)–O(6)	1.803(3)
Lu(1)–O(9)	2.212(3)	I(3)–O(7)	1.812(3)
Lu(1)–O(10)	2.315(3)	I(3)–O(8)	1.817(3)
I(1)–O(1)	1.838(3)	I(3)–O(9)	1.803(3)
Angles (deg)			
O(1)–I(1)–O(2)	97.26(13)	O(5)–I(2)–O(6)	97.21(13)
O(1)–I(1)–O(3)	97.31(14)	O(7)–I(3)–O(8)	101.37(14)
O(2)–I(1)–O(3)	99.39(14)	O(7)–I(3)–O(9)	92.77(13)
O(4)–I(2)–O(5)	98.22(14)	O(8)–I(3)–O(9)	98.65(14)
O(4)–I(2)–O(6)	98.08(13)		

Symmetry codes: (a) x, $y-1$, z; (b) x, $1-y$, $1/2+z$.

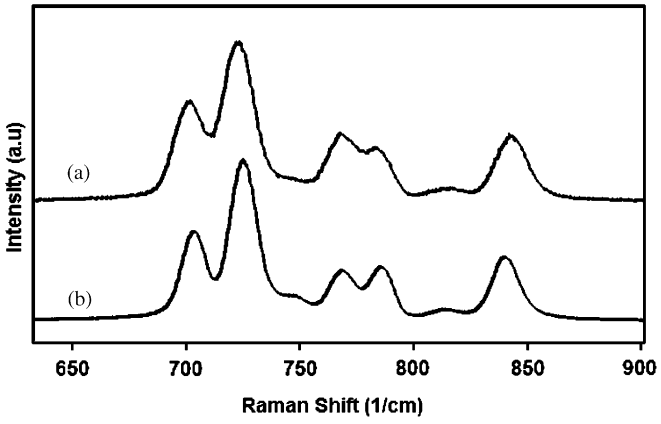

Fig. 6. Raman spectrum of (a) $Lu(IO_3)_3$, and (b) $Yb(IO_3)_3$ at room temperature in the I–O stretching frequency region.

there is only a slight shift in energies. Hence, the corresponding bands are observed at 703 and 725 cm^{-1} with a shoulder at 747 cm^{-1}, a doublet at 768 and 786 cm^{-1}, and at higher energies, there occur a sharp band at 840 cm^{-1} and a weak broad band at 812 cm^{-1}.

Previous interpretations [27–33] of Raman spectra corresponding to the I–O vibrations in iodate salts of trivalent lanthanide and actinide systems are based on the assumption that little inter-ionic coupling exists between the crystallographically unique IO_3^- anions [32–35]. Hence, each of the spectral regions described above can be associated with the unique iodate anions. Within each unique iodate ion the presence of intra-ionic vibrational coupling is dependent on several factors. In previous studies of iodate salts of mono- and divalent cations, systems where one of the I–O bond distances is significantly shorter than the other two distances were found to display

uncoupled symmetric stretching [31–35]. In such instances, the asymmetric component appears at a lower energy when compared to the symmetric stretching frequency. In addition, an intensity comparison can help to differentiate between these two modes as the symmetric component usually displays a more intense band than the asymmetric component.

Each of the three spectral regions shows the presence of weak shoulders and/or components both on the high- and low-energy sides of the most intense bands. Based on this observation lack of intra-ionic coupling cannot be excluded.

The I–O bond distances at the three unique sites are essentially indistinguishable having average values of 1.822, 1.818, and 1.812 Å at I(1), I(2), and I(3) sites, respectively. However, the average O–I–O angle at the I(1) site is smaller as compared with the other two sites (94.4, 97.2, and 97.9 at the I(1), I(2), and I(3) sites, respectively). Following the previous suggestions [31–35], it can be argued that the smaller O–I–O angle at the I(1) site induces a higher frequency shift to the I–O symmetric stretching mode at this site. Hence, the band at 842 cm^{-1} (along with the shoulder at 813 cm^{-1}) is assigned to this site.

The cation interaction with the oxygen atoms at the different iodate sites is used to glean the influence of the lanthanide ion on the frequency of the I–O vibrational profile. The Lu–O distance at the I(1) site is, on average, shorter by ~0.03 and 0.01 Å, as compared to the I(2) and I(3) sites, respectively. Similar differences have been noted previously in the structures of Cm, Am, and Cf iodates [7,8,10]. Thus, it is reasonable to assume that greater electron density is withdrawn from the iodate unit at this site. A consequence is the strengthening of the I–O stretching frequency, which is consistent with the assignment of the highest I–O vibrational band (at 842 cm^{-1}) to the I(1) site.

In Fig. 7, the Raman profiles of the two compounds are shown in the low-energy region covering the bending and lattice vibrational modes. In the I–O stretching region, the two compounds show similar profiles, especially at room temperature, where all the bands match each other. As shown in Fig. 7c for the $Yb(IO_3)_3$ compound, a highly resolved spectrum is obtained upon cooling the material at liquid N_2 temperature. As a result in the 80–500 cm^{-1} region a total of 23 well resolved bands are now observed. The bending mode region (covering 300–500 cm^{-1}), provides a total of 11 well-resolved bands at liquid N_2 temperature compared with the 18 bending modes expected from group theory. The bands below 300 cm^{-1} are assigned to lattice modes. The major bands in $Lu(IO_3)_3$ are observed in similar energy positions, albeit unresolved at room temperature, confirming the structural similarity of the two compounds.

3.3.2. Raman spectra of $Lu(IO_3)_3(H_2O)$ and $Yb(IO_3)_3(H_2O)$

As described earlier, the structural features of these two compounds are dominated by the presence of three

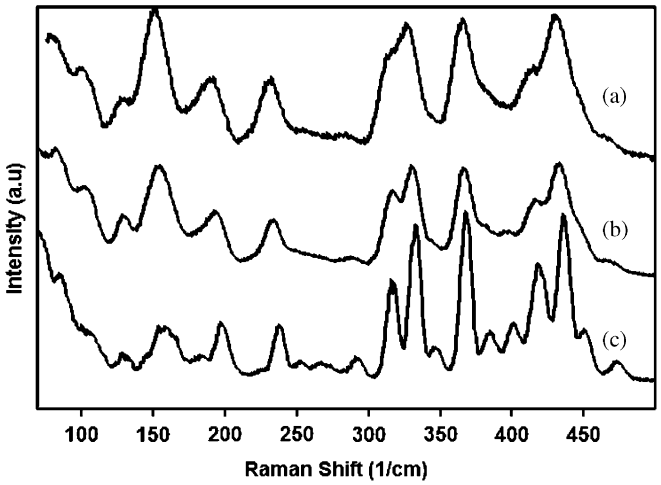

Fig. 7. Raman spectrum of (a) $Lu(IO_3)_3$, and (b) $Yb(IO_3)_3$ at room temperature covering the iodate bending and lattice vibrational regions; (c) Raman spectrum of $Yb(IO_3)_3$ collected at liquid N_2 temperature. A highly resolved spectrum was obtained at low temperature.

crystallographically unique iodate ions. At the I(1) site, two of the oxygen atoms are terminal with only one oxygen coordinated to the metal center. Close inspection of the different interactions at this site indicates that the terminal oxygens are shorter (by ~0.03 Å) than the I–O distances involving the coordinated oxygen atoms. Similarly, at the I(2) site where one of the oxygen atoms (O(6)) is terminal, the I–O distance is shorter by 0.025 Å when compared with that of the two coordinated oxygen atoms. It is only at the I(3) site, where all three oxygens are coordinated, that a more uniform I–O distance is observed. The variations in the I–O interactions are expected to limit intra-ionic coupling of the ν_{I-O} vibrations at least for the I(1) and I(2) sites.

It was stated earlier that the hydrated analogs of Lu- and Yb-iodates have significantly different structural features as compared with the anhydrous compounds. The consequences of these structural differences on the Raman profile are demonstrated in Fig. 8. Both $Lu(IO_3)_3(H_2O)$ and $Yb(IO_3)_3(H_2O)$ display distinctively different vibrational profiles from their respective anhydrous analogs. Hence, the Raman profile can be used as a complementary diagnostic tool, along with X-ray diffraction, to discern the different structural motifs of the compounds.

In the I–O stretching region of $Lu(IO_3)_3(H_2O)$ (Fig. 8a) the most intense band is observed at 742 cm^{-1}; a shift to higher frequency by ~20 cm^{-1} when compared with the anhydrous analog (723 cm^{-1}). In contrast, the highest Raman band in the spectrum appears at a lower energy (834 cm^{-1}), as compared to the value for the anhydrous $Lu(IO_3)_3$ shown in Fig. 6a. As is the case with the anhydrous system, the monohydrate analogs of both Yb and Lu display similar Raman profiles presumably due to the similarities in size of the metal ions and identical structural features of the two compounds.

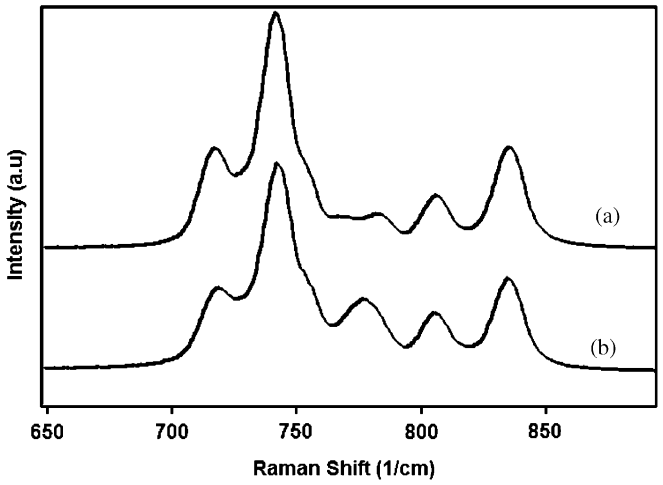

Fig. 8. Raman spectrum of (a) $Lu(IO_3)_3(H_2O)$, and (b) $Yb(IO_3)_3(H_2O)$ at room temperature in the I–O stretching region.

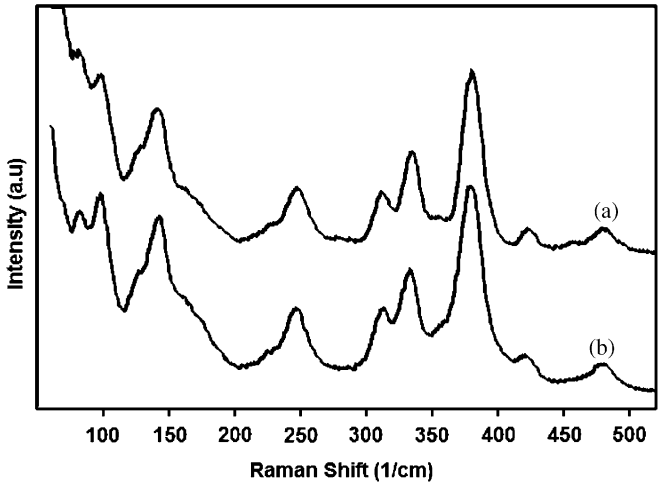

Fig. 9. Raman spectrum of (a) $Lu(IO_3)_3(H_2O)$, and (b) $Yb(IO_3)_3(H_2O)$ at room temperature in the iodate bending and lattice vibrational regions.

The regions covering the bending and lattice modes of these compounds are shown in Fig. 9. The spectral profiles for these regions are quite different from those of the anhydrous compounds, although no significant changes, either in energy positions or relative intensities are evident between the spectra of the two hydrated lanthanide iodates. The bending mode region (300–500 cm^{-1}) consists of significantly fewer Raman bands (about seven bands) as compared with the profiles for the anhydrous compounds, whereas only 8 bands have been observed in the lattice mode region (80–300 cm^{-1}).

4. Conclusion

Four new metal iodates, $Yb(IO_3)_3$, $Lu(IO_3)_3$, $Yb(IO_3)_3(H_2O)$, and $Lu(IO_3)_3(H_2O)$, have all been isolated as single crystals through the use of hydrothermal reactions. Structural determinations using single-crystal X-ray diffraction have shown that the materials are all alike in that they contain two-dimensional structures; the two anhydrous iodates are isostructural as are the hydrated compounds. These mono-hydrated iodates represent a novel structure type, while the anhydrous compounds crystallize in the $Bi(IO_3)_3$ structure type, as found previously for several other *f*-element iodates. Raman spectra have been collected for all four lanthanide iodates. Although $Yb(IO_3)_3$ and $Lu(IO_3)_3$ show similar profiles due to their isostructural nature, as do $Yb(IO_3)_3(H_2O)$ and $Lu(IO_3)_3(H_2O)$, the differences in the Raman vibrational profiles between the two classes of compounds is significant. Therefore, Raman spectroscopy can be used to discern the different structural motifs of these two classes of materials.

Acknowledgments

Support for this work was provided by the Division of Chemical Sciences, Geosciences and Biosciences, OBES, USDOE, under Contract DE-AC05-00OR22725 with Oak Ridge National Laboratory, managed by UT-Battelle, LLC, and under Grant No. DE-FG02-01ER15187 (to T.E.A.-S.). Dr. Radu Custelcean and Dr. Bruce Moyer are thanked for their generous allocation of X-ray diffractometer time. This research was supported in part by an appointment (R.E.S.) to the Oak Ridge National Laboratory Postdoctoral Research Associates Program administered jointly by the Oak Ridge Institute for Science and Education and Oak Ridge National Laboratory.

References

[1] S.C. Abrahams, J.L. Bernstein, K. Nassau, J. Solid State Chem. 16 (1976) 173.
[2] S.C. Abrahams, J.L. Bernstein, Solid State Comm. 27 (1978) 973.
[3] S.C. Abrahams, J.L. Bernstein, J. Chem. Phys. 69 (1978) 2505.
[4] R. Liminga, S.C. Abrahams, J.L. Bernstein, J. Chem. Phys. 62 (1975) 755.
[5] A.L. Hector, W. Levason, M. Webster, Inorg. Chim. Acta 298 (2000) 43.
[6] R. Liminga, S.C. Abrahams, J.L. Bernstein, J. Chem. Phys. 67 (1977) 1015.
[7] R.E. Sykora, Z. Assefa, R.G. Haire, T.E. Albrecht-Schmitt, Inorg. Chem. 44 (2005) 5667.
[8] R.E. Sykora, Z. Assefa, R.G. Haire, T.E. Albrecht-Schmitt, J. Solid State Chem. 177 (2004) 4413.
[9] X. Chen, H. Xue, X. Chang, H. Zang, W. Xiao, J. Alloys Compd. 398 (2005) 173.
[10] R.E. Sykora, Z. Assefa, R.G. Haire, T.E. Albrecht-Schmitt, Inorg. Chem. 45 (2006) 475.
[11] P. Douglas, A.L. Hector, W. Levason, M.E. Light, M.L. Matthews, M. Webster, Z. Anorg. Allg. Chem. 630 (2004) 479.
[12] A.L. Hector, S.J. Henderson, W. Levason, M. Webster, Z. Anorg. Allg. Chem. 628 (2002) 198.
[13] P.K. Sen Gupta, H.L. Ammon, S.C. Abrahams, Acta Crystallogr. C 45 (1989) 175.
[14] W. Runde, A.C. Bean, B.L. Scott, Chem. Comm. (2003) 1848.
[15] R.W. Stoughton, R. B. Duffield, US Patent No. 2,856,261, 1958.

[16] B.A. Fries, US Patent No. 2,926,067, 1960.
[17] B. Weaver, Anal. Chem. 40 (1968) 1894.
[18] B. Bentria, D. Benbertal, M. Bagieu-Beucher, R. Masse, A. Mosset, J. Chem. Crystallogr. 33 (2003) 867.
[19] A.C. Bean, S.M. Peper, T.E. Albrecht-Schmitt, Chem. Mater. 13 (2001) 1266.
[20] T.E. Albrecht-Schmitt, P.M. Almond, R.E. Sykora, Inorg. Chem. 42 (2003) 3788.
[21] W. Runde, A.C. Bean, T.E. Albrecht-Schmitt, B.L. Scott, Chem. Comm. (2003) 478.
[22] SADABS, Acta Crystallogr. A 51 (1995) 33.
[23] G.M. Sheldrick, SHELTXL PC, version 5.0, An integrated system for solving, refining, and displaying crystal structures from diffraction data, Siemens Analytical X-ray Instruments, Inc., Madison, WI, 1994.
[24] R.E. Sykora, A.C. Bean, B.L. Scott, Wolfgang Runde, T.E. Albrecht-Schmitt, J. Solid State Chem. 177 (2004) 725.
[25] R.E. Sykora, S.M. McDaniel, D.M. Wells, T.E. Albrecht-Schmitt, Inorg. Chem. 41 (2002) 5126.
[26] N.E. Brese, M. O'Keeffe, Acta. Crystallogr. B 47 (1991) 192.
[27] A.C. Bean, B.L. Scott, T.E. Albrecht-Schmitt, W. Runde, Inorg. Chem. 42 (2003) 5632.
[28] G. Pracht, N. Lange, H.D. Lutz, Thermochim. Acta 13 (1997) 293.
[29] H.D. Lutz, E. Alici, Th. Kellersohn, J. Raman Spectrosc. 21 (1990) 387.
[30] J.R. During, O.D. Bonner, W.H. Breazeale, J. Phys. Chem. 69 (1965) 3886.
[31] V. Schellenschlager, G. Pracht, H.D. Lutz, J. Raman Spectrosc. 32 (2001) 373.
[32] H.D. Lutz, E. Suchanek, Spectrochim. Acta A 56 (2000) 2707.
[33] G. Pracht, R. Nagel, E. Suchanek, N. Lange, H.D. Lutz, Z. Anorg. Allg. Chem. 624 (1998) 1355.
[34] H.D. Lutz, H. Christian, W. Eckers, Spectrochim. Acta A 41 (1985) 637.
[35] H.D. Lutz, T. Kellersohn, B. Müller, J. Henning, Spectrochim. Acta A 44 (1988) 497.